Journal of
Marine Science and Engineering

MDPI

Article

Determining the Horizontal and Vertical Water Velocity Components of a Turbulent Water Column Using the Motion Response of an Autonomous Underwater Vehicle

Supun A. T. Randeni P. [1,*], Alexander L. Forrest [1,2], Remo Cossu [1,3], Zhi Q. Leong [1] and Dev Ranmuthugala [1]

1 Australian Maritime College, University of Tasmania, Launceston, Tasmania 7250, Australia; alforrest@ucdavis.edu (A.L.F.); r.cossu@uq.edu.au (R.C.); zhi.leong@utas.edu.au (Z.Q.L.); D.Ranmuthugala@amc.edu.au (D.R.)
2 Department of Civil and Environmental Engineering, University of California—Davis, Davis, CA 95616, USA
3 Department of Civil Engineering, University of Queensland, Brisbane, Queensland 4072, Australia
* Correspondence: Supun.Randeni@utas.edu.au; Tel.: +61-47-047-6942

Received: 18 May 2017; Accepted: 28 June 2017; Published: 4 July 2017

Abstract: This work introduces a new method to calculate the water velocity components of a turbulent water column in the x, y, and z directions using Autonomous Underwater Vehicle (AUV) motion response (referred to as the 'WVAM method'). The water column velocities were determined by calculating the difference between the motion responses of the vehicle in calm and turbulent water environments. The velocity components obtained using the WVAM method showed good agreement with measurements from an acoustic Doppler current profiler (ADCP) mounted to the AUV. The standard deviation between the two datasets were below 0.09 m s^{-1} for the velocity components in the x, y, and z directions, and were within the uncertainty margin of the ADCP measurements. With the WVAM method, it is possible to estimate the velocity components within close proximity to the AUV. This region encompasses the vehicle boundary layer and the ADCP blanking distance, which is not typically resolved. Estimating vertical and horizontal velocities around the boundary layer of the AUV is important for vehicle navigation and control system optimization, and to fill the blanking distance gap within a water column velocity profile, which is important for flow field characterization. The results show that it is possible to estimate the flow field in the vicinity of AUVs and other self-propelled vehicles.

Keywords: autonomous underwater vehicles; acoustic Doppler current profilers; water column velocities; hydrodynamic coefficients; system identification

1. Introduction

Measuring water column velocities is an essential component of physical oceanographic surveys but is also important for many applications, such as determining sediment transport [1] and assessing the turbulent flux in the surface mixed layer [2]. Conventionally, broadband acoustic Doppler current profilers (ADCPs) are used to measure water column velocity profiles using the Doppler frequency shift of a sound wave transmitted by the device resulting from particles in the water column moving with the fluid [3]. Stationary ADCPs can be used to determine flow profiles at a fixed location. The spatial and temporal distributions of velocity fields can be potentially determined with an array of such devices; however, the associated costs may restrict the number of sensors, limiting the spatial resolution of the measured velocity profiles.

An alternative is to install similar instrumentation on mobile platforms to map the three dimensional water velocity components with a higher spatial resolution, although it is difficult to capture time series information with these vehicles [4]. At larger water depths, subsea mobile platforms, such as autonomous underwater vehicles (AUVs), provide increased potential for such surveys that are logistically not possible using surface-borne techniques. AUVs are more reliable to undertake missions in areas logistically difficult or inaccessible for surface vessels and other types of underwater vehicles such as remotely-operated vehicles (ROVs) and manned submersibles. For this reason, combined with the relative stability of the vessel and being decoupled from surface noise and reflectance, AUV mounted ADCPs have been adopted to measure water column velocities [5,6].

Acoustic Doppler current profilers have a blanking distance in proximity to the device whose size depends on the frequency of the instrument in which the flow velocity data is not resolved [3]. Larger AUVs tend to have low frequency ADCPs to obtain a larger range; however, it also increases the size of the blanking distance. For example, 150 kHz ADCPs have a maximum range of around 200 m and a blanking distance of around 2–3 m, while the maximum range and blanking distance of 1200 kHz ADCPs are around 20 m and 0.5–1 m respectively. Gandhi et al. [7] utilised a power-law relation to interpolate the water velocity profile for the blanking distance near the sensor when determining discharge measurements in small hydropower stations in order to reduce the error due to the blanking distance. However, such interpolations are invalid in unstructured flow fields.

Previously, Hayes and Morison [2] introduced a new technique to determine the turbulent vertical water velocities, and fluxes of heat and salt using the AUV motion data. A horizontal profile of vertical water velocity was obtained by applying a Kalman filter to the AUV motion data. However, it cannot be readily adopted for commercial AUVs due to the modelling complexity and the requirement of the typically unavailable vehicle control law algorithm. Frajka-Williams et al. [8] developed a technique to estimate vertical water velocities from Seaglider autonomous underwater gliders, produced by Kongsberg Maritime AS, Kongsberg, Norway, using the difference between a predicted glider flight speed in still water and the observed glider vertical velocity from pressure. Rudnick et al. [9] determined the vertical water velocity from Spray gliders using two methods; first, using a model approach similar to the Frajka-Williams, Eriksen, Rhines and Harcourt [8]. The second approach was to high-pass the measured vertical velocity of the vehicle under the assumption that changes in glider flights are low frequency compared to the water velocities. All three of these methods were limited to the vertical water velocity.

This study introduces a method to calculate the water velocity components in the x, y, and z directions of a turbulent water column using the AUV motion response (hereinafter referred to as the 'WVAM method'). The WVAM method determines the fine scale variations of water velocities (with a smallest measurable length scale of around 2.7 m in the current vehicle configuration) by comparing the motion response of the vehicle when operating within turbulent and calm water environments respectively. The key advantage of the WVAM method is that it provides velocity estimates within the blanking distance of the ADCP and the associated vehicle boundary layer which are usually unknown based on previous methods. The following sections of the article provide an overview of the experimental tools, test field details and novel methodologies employed for this work. Subsequently, the assessment and discussion of the validation and verification of the WVAM method are presented. Potential applications of the WVAM method and possible future developments are discussed in the Recommendations section.

2. Materials and Procedures

2.1. Instrumentation

A Gavia-class modular AUV (built by Teledyne Gavia ehf., Kópavogur, Iceland) [10] was used to test and validate the proposed WVAM method. As configured for testing, this vehicle consists of a nose cone module, battery module, GeoSwath Plus Kongsberg Maritime AS (Kongsberg,

Norway) interferometry sonar module, 1200 kHz Teledyne RD Instruments (San Diego, CA, USA) ADCP/Doppler velocity log (DVL) module, Kearfott (NJ, USA) T24 inertial navigation system (INS) module, control module, and a propulsion module (Figure 1). The overall length of the vehicle was 2.7 m, the diameter was 0.2 m, and the dry weight in air was approximately 70 kg. The Kearfott T24 INS, aided with velocity over ground measurements obtained from the DVL bottom-tracking mode, was utilized by the AUV to determine position of the AUV and vehicle velocities in six-degree-of-freedom (6-DOF). The depth of the vehicle was obtained from the Keller (Winterthur, Switzerland) Series 33Xe pressure sensor on-board the AUV. These sensor measurements were recorded in the vehicle log at a frequency of 0.87 Hz.

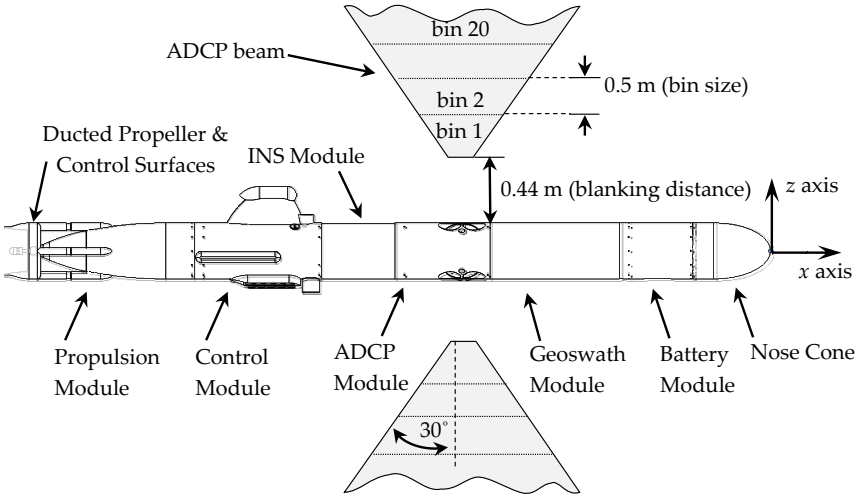

Figure 1. Configuration of the utilised Gavia AUV with the ADCP beam geometry as indicated.

AUVs are preprogramed to follow a pre-set mission route with a given surge speed. When an AUV is operating in an environment with highly-fluctuating water velocities (e.g., in a turbulent water column), the forces induced by these velocities can interrupt the control stability and change the vehicle speed, depth, pitch, and yaw angles (i.e., motion response of the AUV) from the pre-set values. In order to compensate for such changes in performance, the vehicle's dynamic control system adjusts the revolution speed of the propeller and the angles of the four control surfaces located at the stern of the propulsion module. According to these adjustments, the motion response of the AUV will change and the AUV will target the initially-prescribed mission track [11] unless the propeller and the control surfaces are unable to cope with the external forces.

The ADCP module of the AUV included two 1200 kHz Teledyne RD Instruments ADCPs/DVLs arranged in upward- and downward-looking configurations. While the upward-looking transducers were configured so that the instrument only collected water column velocity data relative to the AUV, the downward-looking set had a dual purpose: (i) water column data collection (i.e., ADCP mode), and (ii) estimation of the velocity of the vehicle relative to the ground as an input into the navigation solution of the vehicle (i.e., DVL mode). At every sampling time-step, the instrument's mode of operation switched between the ADCP and DVL. The ADCPs were programmed to profile approximately 10 m of water column in 0.5 m range bins so that the three directional water velocity components relative to the AUV in the body-fixed coordinate system are measured in each bin. During post processing, water velocity components relative to the AUV were converted to the Earth-relative velocities by using the vehicle's Earth-referenced velocity measurements from the DVL-aided INS. However, the water velocity measurements remained in the body-fixed coordinate system.

In front of the ADCP transducers (both above and below) there was a blanking distance of 0.44 m (shown in Figure 1). This blanking distance (i.e., a vertical extent away from the vehicle where no velocity measurements are made) exists as transducers are required to recover electronically from the

transmit pulse and to prepare to receive the return signal [3]. An ADCP requires only three transducer beams to acquire the three dimensional water velocity components. The fourth redundant transducer evaluates the quality of the velocity measurements by comparing two estimations of the vertical water velocity. The difference between the two is called the error velocity [12].

2.2. Site Description

The objective of this study was to derive the WVAM method that calculates the velocity components of a water column by comparing the motion response of the vehicle when operating within a turbulent environment and a simulated calm water environment. The determined velocities are validated with the velocity measurements from the on-board ADCP. Field tests were carried out at two locations in Tasmania, Australia—in Lake Trevallyn (a low energy system with average flows at <0.05 m s^{-1}) to develop the calm water based simulation model and in the Tamar estuary (a high energy system with peak flows at 2 m s^{-1}) to test the WVAM method (Figure 2a).

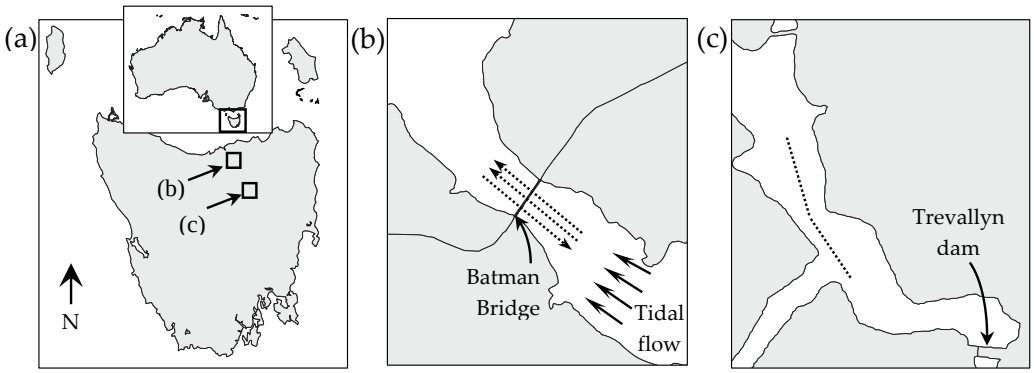

Figure 2. (**a**) The two experimental field sites in Tasmania, Australia (inset). (**b**) The Batman Bridge site with the direction of dominant tidal current flow as shown with solid straight-line arrows. AUV tracks are illustrated with dotted arrows. (**c**) The Lake Trevallyn site with low turbulence conditions. AUV missions were conducted along the dotted line.

The main field study was conducted in the Tamar estuary near the Batman Bridge (Figure 2b) on 14 June 2014. The width of the estuary narrows down to less than 300 m near the Batman Bridge, which causes highly turbulent flow conditions along the main channel axis, as shown in Figure 2b. In addition, varying bathymetry of the estuary (i.e., the 35 m depth at the north-west end of the test location reduces to 15 m near the bridge and increases again to 30 m at the opposite end) induces further constraints to the tidal flow. As a result of the narrowing and flow construction, this section of the estuary usually exhibits strong tidal currents (with maximum flow of >2 m s^{-1}) and water level fluctuations of around 3 m [13]. Three straight-line AUV runs were conducted along, and against, the tidal flow direction (see Figure 2b), maintaining a constant altitude of 10 m above the bottom, and a propeller speed of 700 revolutions per min (RPM). These missions were used to determine the water column velocities using the WVAM method.

A series of manoeuvres was conducted in Lake Trevallyn, Tasmania (Figure 2c) between 30 October and 14 November 2013 to derive the hydrodynamic coefficients of the AUV using a system identification approach. The manoeuvres included straight-line runs conducted for five different propeller speeds (i.e., 525 RPM, 600 RPM, 675 RPM, 750 RPM, and 825 RPM) and a zig-zag manoeuvre in yaw and pitch planes by changing the coordinate waypoints and operating depths concurrently. The manoeuvres were designed to stimulate the vehicle dynamics in vertical as well as horizontal planes, which is critical for accurate estimation of simulation model parameters. The water depth of the test site was greater than 6 m and surface wave heights were below 50 mm. The AUV missions were carried out between 2 and 4 m below the free surface to minimize the surface wave formation and the interaction effects with the lake bottom [14,15]. During the manoeuvres, the vehicle's ADCP recorded

minor variations of the water column velocities with averaged values in the surge, sway, and heave directions of less than 0.05 m s^{-1}. These minor water velocities indicate a calm water environment. The AUV missions were conducted along the dotted line shown in Figure 2c.

2.3. WVAM Method

The WVAM method (Figure 3) starts with the AUV undergoing a straight-line, constant altitude mission through a region where the water column velocities are to be measured (i.e., in the turbulent water column). The vehicle's control system provides necessary commands to the propulsion motor and control surfaces (i.e., the propeller RPM commands and the control surface angle commands) to overcome the disturbances from the turbulent flow and to continue the prescribed straight-line path while maintaining a constant altitude set point. These control commands, recorded in the vehicle log, are then executed with the simulation model that represents a calm water environment. Since there are no currents and flow disturbances in the simulated calm water condition, the vehicle velocities from the simulation model will be different to the actual velocities measured from the DVL aided INS of the AUV. The difference between the two motion responses provides a measurement of the water column velocities relative to the ground. Equation (1) gives water velocity calculation in the general form. The requirement of the calm water manoeuvres is for initial development of the simulation model, which is applicable for a given vehicle configuration.

$$\vec{\nu}_{\text{water(t)}} = \vec{\nu}_{\text{AUV(turbulent)(t)}} - \vec{\nu}_{\text{AUV(calm)(t)}} \quad (1)$$

where, $\vec{\nu}_{\text{water}}$ is the linear velocity vector of the surrounding water column (along the x, y, and z directions) relative to the earth in the body-fixed coordinate system (see Figure 4), $\vec{\nu}_{\text{AUV(turbulent)}}$ is the linear velocity vector of the AUV relative to the Earth measured in the turbulent environment using the DVL-aided INS, and $\vec{\nu}_{\text{AUV(calm)}}$ is the linear velocity vector obtained from the calm water simulation model when the control commands recorded during the field tests were simulated. Subscript t indicates the time-step.

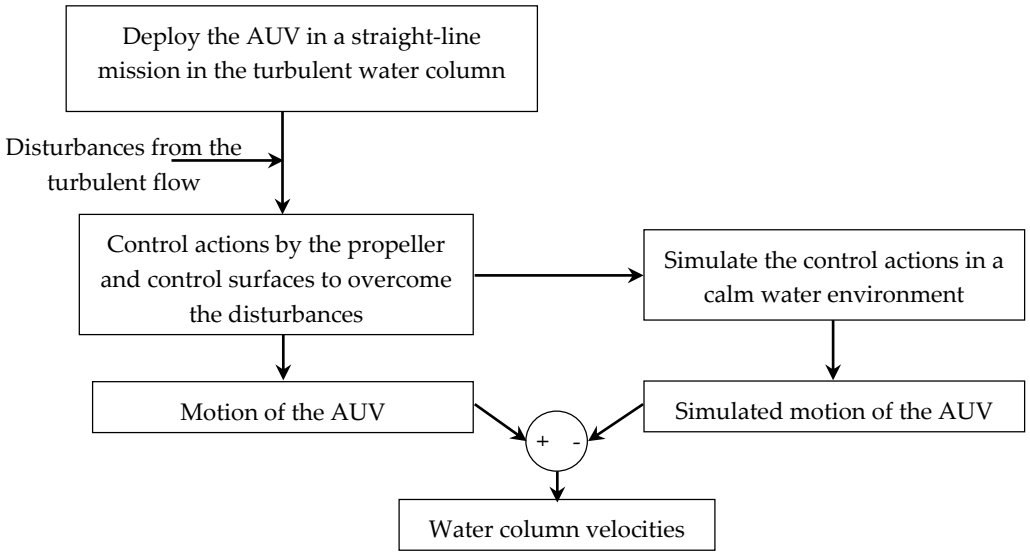

Figure 3. The WVAM method flowchart to predict water column velocities from the observed vehicle motions. As given in Equation (1), the difference between the motion responses in the turbulent (i.e., experimental) and calm (i.e., simulated) water flow condition provides a measurement of the water column velocities relative to the ground.

The AUV is required to be assumed as a particle if infinitely small water column velocity fluctuations are measured using Equation (1). However, an AUV is not sufficiently small in

size to be assumed as a particle; therefore, due to the length of the vehicle, the water column velocity measurements derived from Equation (1) is restricted in terms of the length scale resolution. The minimum measurable velocity variation length scale is also limited by the sensor sampling frequency. This is further discussed in the Discussion section.

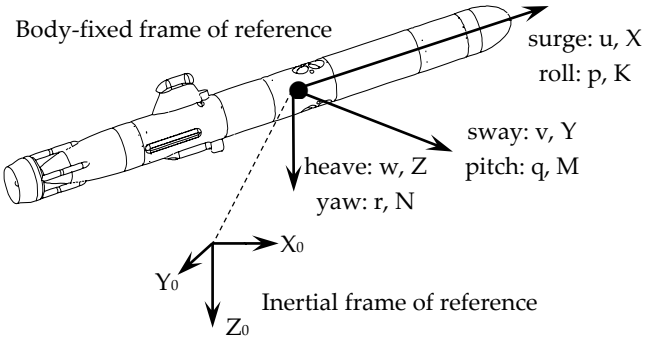

Figure 4. Inertial and body-fixed frames of reference. The origin of the body fixed coordinate system was at the centre of buoyancy of the vehicle (marked by the filled circle).

2.3.1. AUV Simulation Model

The motion simulation model of the Gavia AUV was developed to reproduce the vehicle's linear velocities in a calm water environment in response to the time series of the control commands. This included the propeller RPM command which was a direct input into the simulator. In order to simplify and reduce the associated uncertainties, the time series of pitch angle (θ), pitch rate (q), pitch acceleration ($\dot{q}$), yaw rate (r), and yaw acceleration ($\dot{r}$) values recorded during the physical runs (i.e., measured by the gyroscopic sensors within the INS) were given as inputs to the simulator instead of providing the associated control surface angle commands. This simplification avoided the requirement of determining the control surface forces and moments, and using them to derive the rolling, pitching and yawing motions as the actual vehicle attributes were provided as inputs to the simulator. Therefore, the mathematical model was able to be limited to 3-DOF (i.e., linear motions along the x, y, and z directions), thereby eliminating the requirement to model the angular motions of the vehicle.

The simulation model was developed using MATLAB Simulink software (developed by Mathworks, MA, USA) by modelling the rigid body dynamics and hydrodynamics of the vehicle in accordance with Fossen [16] for AUV dynamics and Prestero [17] for the simulation model. The 6-DOF motion of an underwater vehicle can be described using the equations of motion given in Equation (2), in the vectorial form [16]. The mathematical formulae presented in this paper are based on the Society of Naval Architects and Marine Engineers (SNAME) [18] notation with the associated coordinate system given in Table 1 and Figure 4. The Earth-fixed frame of reference was used as the inertial reference. The origin of the body-fixed reference frame was at the centre of buoyancy of the vehicle, which is located at the ADCP module as shown in Figure 4.

$$\mathrm{M}\dot{\vec{\nu}} + \mathrm{C}\left(\vec{\nu}\right)\vec{\nu} + \mathrm{D}\left(\vec{\nu}\right)\vec{\nu} + \mathrm{g}\left(\vec{\eta}\right) = \tau_{\text{control}} \tag{2}$$

where, M is the system inertia matrix, $\mathrm{C}\left(\vec{\nu}\right)$ is the Coriolis-centripetal matrix, $\mathrm{D}\left(\vec{\nu}\right)$ is the damping matrix, $\mathrm{g}\left(\vec{\eta}\right)$ is the vector of the gravitational/buoyancy forces and moments, τ_{control} is the vector of propulsion, control surface forces, and moments, $\vec{\nu}$ is the velocity vector (i.e., [u, v, w, p, q, r] where p, q, and r are the angular velocities around the x, y, and z axes), and $\vec{\eta}$ is the vector of position/Euler angles (i.e., [x, y, z, ϕ, θ, ψ] where ϕ, θ and ψ are the roll, pitch, and yaw angles respectively). M and

$C\left(\overrightarrow{\nu}\right)$ are further expanded in Equations (3) and (4), where, M_{RB} and $C_{RB}\left(\overrightarrow{\nu}\right)$ are the rigid body force components of M and $C\left(\overrightarrow{\nu}\right)$ matrices, while M_A and $C_A\left(\overrightarrow{\nu}\right)$ are their added mass components.

$$M = M_{RB} + M_A \tag{3}$$

$$C\left(\overrightarrow{\nu}\right) = C_{RB}\left(\overrightarrow{\nu}\right) + C_A\left(\overrightarrow{\nu}\right) \tag{4}$$

Table 1. The 6-DOF notation system.

Degree-of-Freedom	Forces & Moments	Linear & Angular Velocity	Position & Euler Angles
Motions in the x-direction (surge)	X	u	x
Motions in the y-direction (sway)	Y	v	y
Motions in the z-direction (heave)	Z	w	z
Rotation about the x-axis (roll)	K	p	φ
Rotation about the y-axis (pitch)	M	q	θ
Rotation about the z-axis (yaw)	N	r	ψ

The 6-DOF force and moment matrices that appear in Equation (2) are given in Fossen [16] in their full form. In this study, Equation (2) has been reduced to 3 DOF (i.e., to equations of motion in x, y and z directions) and simplified assuming the products of inertia (i.e., I_{xy}, I_{xz} and I_{yz}) are zero since they are negligibly small compared to the moments of inertia (i.e., I_{xx}, I_{yy}, and I_{zz}) of the vehicle [17]. Equations (5)–(7) represent the expanded forms of Equation (2) in the respective directions of x, y, and z. The left-hand sides of the equations demonstrate the rigid body dynamics and added mass terms while the right-hand sides show the hydrostatic, hydrodynamic damping, and control forces [17]. The hydrodynamic coefficients are non-dimensionalised according to prime-system I notation [19] using 2.7 m as the vehicle length (L), 1000 kg m^{-3} as the fresh water density, and 2 m s^{-1} as the prescribed forward speed (U) . The notation of the hydrodynamic coefficients presented in the equations below follow SNAME [18]. For example, $X_{u|u|}$ is the partial derivative of the surge force (X) with respect to the square of the surge speed ($u|u|$); i.e., $X_{u|u|} = \partial X/\partial(u|u|)$. $X'_{u|u|}$ represents the non-dimensionalised coefficient.

$$\begin{gathered}\tfrac{\rho}{2}L^3\left[\left(\tfrac{2}{\rho L^3}m - X'_{\dot{u}}\right)\dot{u}\right] + mz_g\dot{q} - my_g\dot{r} = -(W-B)\sin(\theta) + \tfrac{\rho L^2}{2U}\left[X'_{uuu}u^3\right] + \tfrac{\rho}{2}L^2\left[X'_{u|u|}u|u|\right] + \\ \tfrac{\rho}{2}L^2U\left[X'_u u\right] + \tfrac{\rho}{2}L^3\left[\left(X'_{wq} - \tfrac{2}{\rho L^3}m\right)wq + \left(X'_{vr} + \tfrac{2}{\rho L^3}m\right)vr\right] + X_n \times RPM^2\end{gathered} \tag{5}$$

$$\begin{gathered}\tfrac{\rho}{2}L^3\left(\tfrac{2}{\rho L^3}m - Y'_{\dot{v}}\right)\dot{v} - mz_g\dot{p} + \tfrac{\rho}{2}L^4\left(\tfrac{2}{\rho L^4}mx_g - Y'_{\dot{r}}\right)\dot{r} = +\tfrac{\rho}{2}L^2\left[Y'_{v|v|}v|v|\right] + \\ \tfrac{\rho}{2}L^2U\left[Y'_v v\right] + \tfrac{\rho}{2}L^3U\left[Y'_p p\right] + \tfrac{\rho}{2}L^3U\left[Y'_q q\right] + \tfrac{\rho}{2}L^3U\left[Y'_r r\right]\end{gathered} \tag{6}$$

$$\begin{gathered}\tfrac{\rho}{2}L^3\left[\left(\tfrac{2}{\rho L^3}m - Z'_{\dot{w}}\right)\dot{w}\right] + my_g\dot{p} - \tfrac{\rho}{2}L^4\left[\left(\tfrac{2}{\rho L^4}mx_g + Z'_{\dot{q}}\right)\dot{q}\right] = (W-B)\cos(\theta) + \\ \tfrac{\rho}{2}L^2\left[Z'_{w|w|}w|w|\right] + \tfrac{\rho}{2}L^2U\left[Z'_w w\right] + \tfrac{\rho}{2}L^3U\left[Z'_p p\right] + \tfrac{\rho}{2}L^3U\left[Z'_q q\right] + \tfrac{\rho}{2}L^3U\left[Z'_r r\right]\end{gathered} \tag{7}$$

where RPM is the vehicle's propeller revolutions per minute and X_n is the thrust coefficient, which is 95×10^{-6} for the Gavia AUV according to the estimation by Thorgilsson [20].

Equations (5)–(7) were rearranged and parameterised to the forms given in Equations (8)–(10) in order to calculate the instantaneous linear accelerations of the AUV in x, y, and z directions, where α' β', and γ' are unknown parameters to be identified using system identification. The physical properties of the AUV, such as the mass, positive buoyancy force, and distances to the vehicle centre of gravity, were superimposed within the parameters, eliminating the requirement to measure them.

$$\begin{gathered}\dot{u} - X_n RPM^2 = \alpha'_1\left[\tfrac{2}{\rho L^3}\sin(\theta)\right] + \alpha'_2\left[\tfrac{1}{UL}u^3\right] + \alpha'_3\left[\tfrac{1}{L}u|u|\right] + \\ \alpha'_4\left[\tfrac{U}{L}u\right] + \alpha'_5[wq] + \alpha'_6[vr] + \alpha'_7\left[\tfrac{2}{\rho L^3}\dot{q}\right] + \alpha'_8\left[\tfrac{2}{\rho L^3}\dot{r}\right]\end{gathered} \tag{8}$$

$$\dot{v} = \beta'_1\left[\frac{1}{L}v|v|\right] + \beta'_2\left[\frac{U}{L}v\right] + \beta'_3[Up] + \beta'_4[Uq] + \beta'_5[Ur] + \beta'_6\left[\frac{2}{\rho L^3}\dot{p}\right] + \beta'_7\left[L\dot{r}\right] \quad (9)$$

$$\dot{w} = \gamma'_1\left[\frac{2}{\rho L^3}\cos(\theta)\right] + \gamma'_2\left[\frac{1}{L}w|w|\right] + \gamma'_3\left[\frac{U}{L}w\right] + \gamma'_4[Up] + \gamma'_5[Uq] + \gamma'_6[Ur] + \gamma'_7\left[\frac{2}{\rho L^3}\dot{p}\right] + \gamma'_8\left[L\dot{q}\right] \quad (10)$$

As shown in the simulation model flowchart given in Figure 5, the instantaneous linear acceleration components of the current time-step is solved using the recorded input parameters (i.e., propeller RPM, θ, q, r, $\dot{q}$, and $\dot{r}$) corresponding to the current time-step and linear vehicle velocities of the previous time-step. The calculated accelerations are then integrated with respect to time to obtain the linear velocity components in the body-fixed reference frame (i.e., u, v, and w), which is the key objective of the simulation model. These velocity components are also used as the input velocities for the future time-step.

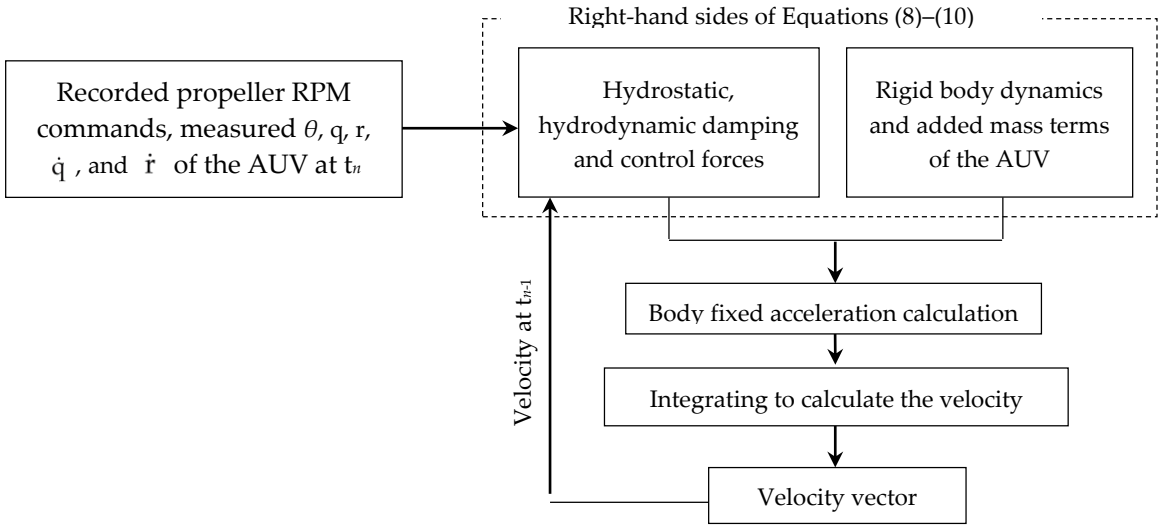

Figure 5. Simulation model flowchart. The acceleration vector of the current time-step is solved using the velocity vector from the previous time-step and commanded propeller RPM while θ, q, r, $\dot{q}$, and $\dot{r}$ are subsequently replaced with the values recorded during field tests. The body-fixed velocity vector was obtained by integrating the acceleration vector with respect to time.

2.3.2. System Identification

The simulation model requires an accurate representation of the associated system parameters to precisely predict the motion of the AUV. Identification of the parameters was conducted in the MATLAB Simulink environment using the recursive least squares estimation block set of the MATLAB System Identification toolbox, which utilises the theoretical approach outlined in Ljung [21]. Equations (8)–(10) were modified to the format given in Equation (11):

$$y_{(t)} = H_{(t)}\Theta_{(t)} \quad (11)$$

where, $y_{(t)}$, $H_{(t)}$ and $\Theta_{(t)}$ vectors are as defined in Table 2 for models in x, y, and z directions.

The unknown parameter vectors (i.e., $\Theta_{(t)}$) were estimated by running the recursive least squares algorithm for the time series motion response data of zig-zag and straight-line manoeuvres conducted at Lake Trevallyn (further information regarding the utilised recursive squares technique could be obtained from Ljung [21]). The values of the identified parameters given in Table 3.

Table 2. $y_{(t)}$, $H_{(t)}$ and $\Theta_{(t)}$ vectors of Equation (11) for x, y, and z directions.

x Direction	*y* Direction	*z* Direction
$y_{(t)} = \dot{u} - X_n RPM^2$	$y_{(t)} = \dot{v}$	$y_{(t)} = \dot{w}$
$H_{(t)} = \begin{bmatrix} \frac{2}{\rho L^3}\sin(\theta) & \frac{1}{L}u\lvert u\rvert \\ wq \quad vr \quad Lq^2 \quad Lr^2 & \frac{2}{\rho L^3}\dot{q} \end{bmatrix}$	$H_{(t)} = \begin{bmatrix} \frac{2}{\rho L^3}qr & \frac{1}{L}v\lvert v\rvert \\ \frac{1}{L}uv \quad ur \quad Lr\lvert r\rvert & L\dot{r} \end{bmatrix}$	$H_{(t)} = \begin{bmatrix} \frac{2}{\rho L^3}\cos(\theta) & \frac{1}{L}w\lvert w\rvert \\ \frac{1}{L}uw \quad uq \quad Lq\lvert q\rvert & L\dot{q} \end{bmatrix}$
$\Theta_{(t)} = \begin{bmatrix} \alpha'_1 & \alpha'_2 & \alpha'_3 & \alpha'_4 \\ \alpha'_5 & \alpha'_6 & \alpha'_7 \end{bmatrix}$	$\Theta_{(t)} = \begin{bmatrix} \beta'_1 & \beta'_2 & \beta'_3 & \beta'_4 \\ \beta'_5 & \beta'_6 \end{bmatrix}$	$\Theta_{(t)} = \begin{bmatrix} \gamma'_1 & \gamma'_2 & \gamma'_3 & \gamma'_4 & \gamma'_5 & \gamma'_6 \end{bmatrix}$

Table 3. $y_{(t)}$, $H_{(t)}$, and $\Theta_{(t)}$ vectors of Equation (11) for x, y, and z directions.

Parameter	Value	Parameter	Value	Parameter	Value
$\alpha'_1 = \frac{-(W-B)}{\left(\frac{2}{\rho L^3}m - X'_{\dot{u}}\right)}$	-2.47×10^4	$\beta'_1 = \frac{Y'_{v\lvert v\rvert}}{\left(\frac{2}{\rho L^3}m - Y'_{\dot{v}}\right)}$	1.20×10^{-1}	$\gamma'_1 = \frac{(W-B)}{\left(\frac{2}{\rho L^3}m - Z'_{\dot{w}}\right)}$	1.53×10^1
$\alpha'_2 = \frac{X'_{uuu}}{\left(\frac{2}{\rho L^3}m - X'_{\dot{u}}\right)}$	-4.64×10^1	$\beta'_2 = \frac{Y'_v}{\left(\frac{2}{\rho L^3}m - Y'_{\dot{v}}\right)}$	-4.91×10^{-2}	$\gamma'_2 = \frac{Z'_{w\lvert w\rvert}}{\left(\frac{2}{\rho L^3}m - Z'_{\dot{w}}\right)}$	-3.72×10^{-2}
$\alpha'_3 = \frac{X'_{u\lvert u\rvert}}{\left(\frac{2}{\rho L^3}m - X'_{\dot{u}}\right)}$	6.02×10^1	$\beta'_3 = \frac{Y'_p}{\left(\frac{2}{\rho L^3}m - Y'_{\dot{v}}\right)}$	4.32×10^{-4}	$\gamma'_3 = \frac{Z'_w}{\left(\frac{2}{\rho L^3}m - Z'_{\dot{w}}\right)}$	-4.69×10^{-2}
$\alpha'_4 = \frac{X'_u}{\left(\frac{2}{\rho L^3}m - X'_{\dot{u}}\right)}$	-4.42×10^1	$\beta'_4 = \frac{Y'_q}{\left(\frac{2}{\rho L^3}m - Y'_{\dot{v}}\right)}$	-3.97×10^{-5}	$\gamma'_4 = \frac{Z'_p}{\left(\frac{2}{\rho L^3}m - Z'_{\dot{w}}\right)}$	3.50×10^{-4}
$\alpha'_5 = \frac{\left(X'_{wq} - \frac{2}{\rho L^3}m\right)}{\left(\frac{2}{\rho L^3}m - X'_{\dot{u}}\right)}$	-7.11	$\beta'_5 = \frac{Y'_r}{\left(\frac{2}{\rho L^3}m - Y'_{\dot{v}}\right)}$	3.78×10^{-4}	$\gamma'_5 = \frac{Z'_q}{\left(\frac{2}{\rho L^3}m - Z'_{\dot{w}}\right)}$	-5.26×10^{-4}
$\alpha'_6 = \frac{\left(X'_{vr} + \frac{2}{\rho L^3}m\right)}{\left(\frac{2}{\rho L^3}m - X'_{\dot{u}}\right)}$	-1.35×10^1	$\beta'_6 = \frac{mz_g}{\left(\frac{2}{\rho L^3}m - Y'_{\dot{v}}\right)}$	2.84×10^1	$\gamma'_6 = \frac{Z'_r}{\left(\frac{2}{\rho L^3}m - Z'_{\dot{w}}\right)}$	5.34×10^{-5}
$\alpha'_7 = \frac{-mz_g}{\left(\frac{2}{\rho L^3}m - X'_{\dot{u}}\right)}$	-8.94×10^2	$\beta'_6 = \frac{-\left(\frac{2}{\rho L^4}mx_g - Y'_{\dot{r}}\right)}{\left(\frac{2}{\rho L^3}m - Y'_{\dot{v}}\right)}$	4.93×10^{-3}	$\gamma'_7 = \frac{-my_g}{\left(\frac{2}{\rho L^3}m - Z'_{\dot{w}}\right)}$	0.00×10^1
$\alpha'_8 = \frac{my_g}{\left(\frac{2}{\rho L^3}m - X'_{\dot{u}}\right)}$	5.21×10^3			$\gamma'_8 = \frac{\left(\frac{2}{\rho L^4}mx_g + Z'_{\dot{q}}\right)}{\left(\frac{2}{\rho L^3}m - Z'_{\dot{w}}\right)}$	-2.17×10^{-3}

The utilised system identification technique is a simple and robust method to determine the mathematical model parameters of a modular AUV, but it has limitations to estimate values for individual hydrodynamic derivatives as several coefficients and vehicle physical properties are overlaid within each parameter. System identification, in general, also has the risk of providing non-physical values for the parameters, limiting the applicability of the parameters to the propeller RPM range, pitch and yaw angle range of the identification manoeuvres. However, similar to most other AUV mapping missions, the AUV is prescribed to run in straight-line paths in the WVAM method, thus requiring the simulations to be conducted generally for straight-line and small pitch and yaw angle (generally below around 8°) manoeuvres, where the hydrodynamic coefficients are within the linear range [22]. The identified parameters obtained from system identification were sufficient for the WVAM method and were verified by simulating a secondary set of manoeuvres conducted in the calm water environment. The results of the verification study is presented in the Assessment section.

3. Assessment

3.1. Validation of the WVAM Method

The WVAM method was validated by comparing the calculated velocity components of the water column with velocity observations obtained with the on-board ADCP. Out of the three straight-line runs conducted at the Batman Bridge site, the one with the largest discrepancy with the ADCP results is presented in Figure 6. The vehicle path was aligned with the predominant tidal flow direction during this run.

Figure 6a compares the vertical velocity response of the AUV (i.e., the velocity component of the AUV in the z direction—w) observed in the turbulent environment (i.e., the Batman Bridge site) with the response obtained from the simulation model representing the calm water. During the experiments, the vertical velocity of the AUV was determined using the DVL-aided INS. Since there are no flow variations in the calm water condition, there is no external forcing on the vehicle. Therefore, the velocity responses from calm and turbulent water surroundings vary from each other. As given in Equation (1), the difference between the two vertical velocity responses provides the vertical water velocity variation along the AUV track at the Batman Bridge site. The horizontal water velocity components in x and y directions were obtained by comparing the vehicle's measured and simulated surge and sway speed responses, respectively.

Figure 6b–d compares the WVAM estimates and ADCP measured water velocity components in the x, y, and z directions, respectively. The ADCP results were smoothed using a moving average filter using a backward scheme with a frame size of six time-steps. The filtered flow velocity components from the first bin of upward and downward looking transducers (i.e., 0.44 m away from the vehicle) were averaged together and taken as the ADCP measurements for the comparison.

The difference between velocities obtained from the WVAM method and the ADCP were calculated by quantifying the standard deviation between the two. The standard deviations of the velocity components in x, y, and z directions were 0.09 m s^{-1}, 0.07 m s^{-1}, and 0.06 m s^{-1}, respectively. The maximum error velocity of the ADCP vertical flow measurements estimated with the redundant transducer was $\pm$0.10 m s^{-1} and Fong and Jones [5] indicated that the velocity measurements taken from an AUV-fixed ADCP typically has an uncertainty margin of $\pm$0.1 m s^{-1}. Thus, the standard deviation of the WVAM method results are within the uncertainty margin of ADCP measurements for x and z directions. The WVAM method provides the water column velocities at the vehicle while the ADCP velocity measurements are the averaged values of the first bins of the upward and downward looking transducers. The WVAM method was further validated by comparing the velocity measured by a stationary upward-looking ADCP moored to the seabed as discussed in Section 4.1.

Since the vehicle was moving against the predominant tidal flow direction, a negative water velocity along the x direction is seen in Figure 6b (positive water velocities were observed when the AUV was running with the flow direction as a result of the inverted body-fixed coordinate system). The best replica between the WVAM and ADCP velocities is noticed in the vertical velocity component. The largest mismatches in velocities along y and z directions are seen at the peaks. The estimated hydrodynamic coefficients of the simulation model using the system identification method could be less accurate for large angles of incidence of the vehicle, where the hydrodynamic forces and moments are in their non-linear ranges. Therefore, as the yaw and pitch angle fluctuations become larger, the accuracy of the simulation model decreases; adversely affecting the WVAM velocity prediction [23]. The disparity at peaks of the velocity components is due to the hydrodynamic coefficients exceeding their linear ranges causing a reduction in the accuracy of the simulation model. Although the peak discrepancy is negligible for the tested runs, it is critical to ensure that the vehicle motion response remains within the applicable range of the hydrodynamic coefficients in order to use the WVAM method. The non-linear hydrodynamic coefficients of an AUV could be obtained more accurately using techniques such as captive model experiments and computational fluid dynamics simulations [24,25].

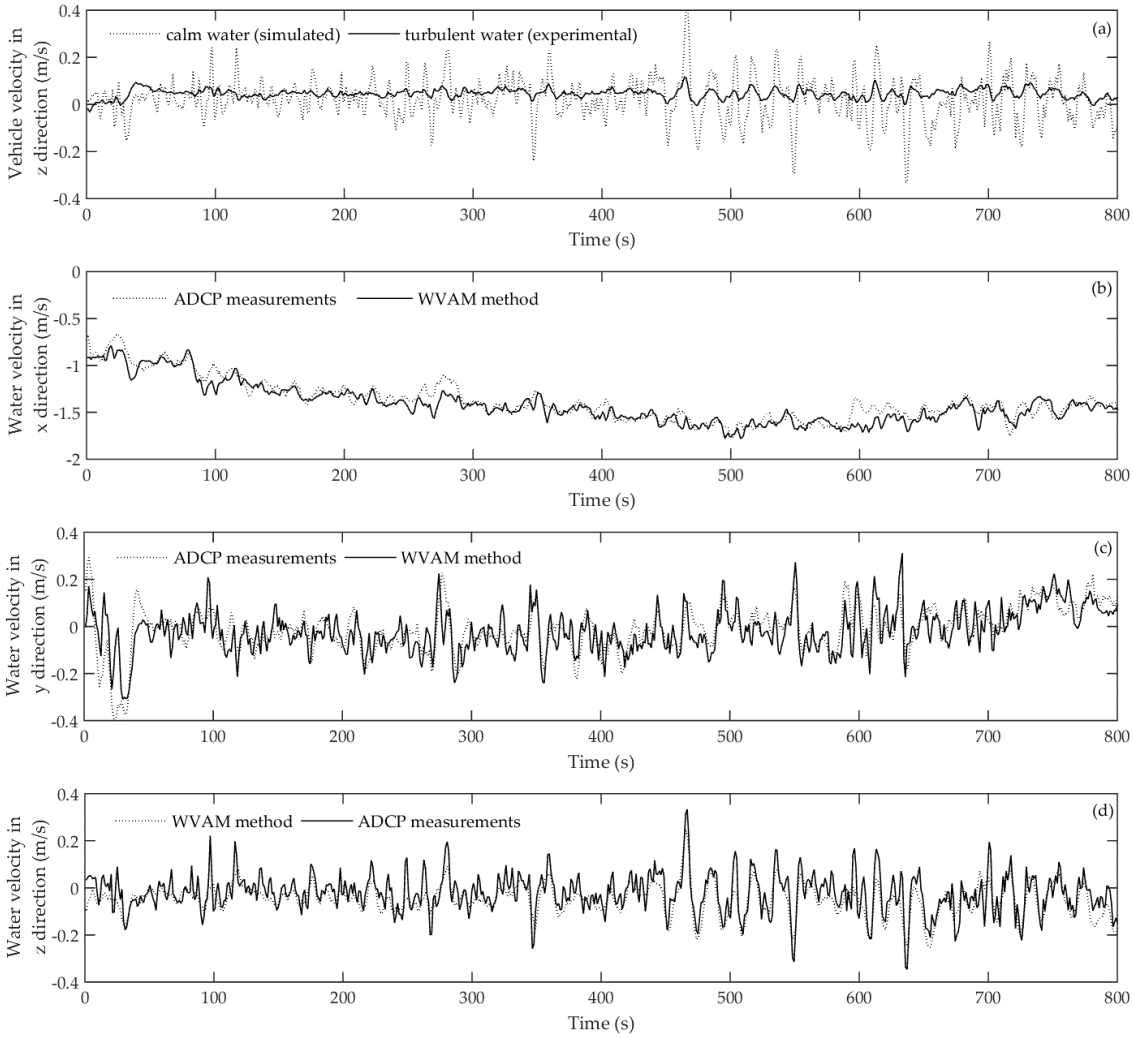

Figure 6. (**a**) The vertical velocity of the vehicle observed in the turbulent (experimental) and calm (simulated) water environments. The difference between the two responses provides the velocity of the water column in the z direction. The comparison between the velocity components of the water column in x, y and z axes (panels (**b**), (**c**), and (**d**), respectively) was calculated using the WVAM method and those obtained from the ADCP measurements smoothed with a moving average filter.

3.2. *Verification of the WVAM Method*

The validation study discussed above demonstrates that the WVAM method is compatible with experimental measurements and could be used to calculate water column velocities in the vicinity of an AUV within the ADCP blanking distance. To gain further confidence, a verification study was conducted to identify the uncertainty margins of the results obtained from this method. The analysis was based on computing the error margins of individual steps, and adding them to obtain the total ambiguity.

The hydrodynamic coefficients of the Gavia AUV for the simulation model were identified by running the recursive least squares algorithm for the time series motion response data collected from the calm water environment at Lake Trevallyn. The uncertainty present in the identified coefficients may affect the water column velocity calculations and therefore it was necessary to quantify the ambiguity of the WVAM method. The performance of the determined coefficients were examined by applying them to the simulation model and simulating a different set of manoeuvres conducted at the Lake Trevallyn site. The AUV runs used for model estimation were not used for this verification process guaranteeing an unbiased verification. The accuracy of the identified coefficients was quantified by

computing the standard deviation between the simulated and actual vehicle velocities in x, y, and z axes, which were 0.010 m s^{-1}, 0.005 m s^{-1}, and 0.002 m s^{-1}, respectively.

During the field tests at the Lake Trevallyn site (i.e., a calm water environment), the on-board ADCP showed minor variations of the water column velocities, with averaged values in the surge, sway and heave directions of less than 0.05 m s^{-1}. These minor water velocities indicate a calm water environment. Nevertheless, there is a minor contribution towards the ambiguity of the results from the WVAM method. Therefore, these velocity components were included in the final uncertainty calculation.

During the experiments, the velocities of the AUV over ground and the pitch and yaw rates were measured using the INS, which was aided with the velocity over ground measurements from the DVL bottom-tracking mode. The uncertainties associated with the DVL-aided INS influence the calm water simulation results, as well as the measurements taken in the turbulent environment. These uncertainties were incorporated twice when calculating the total uncertainty margin of the WVAM method. The uncertainty of the DVL aided Kearfott T24 INS in measuring the speeds over ground is ± 0.05 m s^{-1} [26]. The respective uncertainties of the INS in providing the pitch and yaw rates of the AUV are $\pm 7.96 \times 10^{-5}$ rad s^{-1} and $\pm 1.60 \times 10^{-4}$ rad s^{-1}.

The total uncertainty margin of the WVAM method was determined by adding the individual error components as discussed above and shown in Table 4. Using these values it can be determined that the WVAM method is able to provide velocity components of a turbulent water column in x, y, and z axes with respective uncertainty margins of ± 0.160 m s^{-1}, ± 0.155 m s^{-1}, and ± 0.152 m s^{-1}. In comparison, the uncertainty margins of an ADCP mounted on an AUV and a stationary ADCP in measuring water column velocities is around ± 0.1 m s^{-1} and ± 0.002 m s^{-1}, respectively, for velocity components in the x, y, and z directions.

Table 4. Uncertainty margin of the WVAM method was determined by adding the individual error components of each step.

Uncertainty Components	Uncertainties Along		
	x Direction	y Direction	z Direction
Due to hydrodynamic coefficients	± 0.010 m s^{-1}	± 0.005 m s^{-1}	± 0.002 m s^{-1}
Due to the turbulence present in the calm water environment	± 0.05 m s^{-1}	± 0.05 m s^{-1}	± 0.05 m s^{-1}
Due to sensor errors	± 0.100 m s^{-1}	± 0.100 m s^{-1}	± 0.100 m s^{-1}
Total uncertainty of the WVAM method	± 0.160 m s^{-1}	± 0.155 m s^{-1}	± 0.152 m s^{-1}

4. Discussion

4.1. Accuracy with the Distance from the AUV

The ADCP captures the water velocity components at each bin up to a distance of 10 m away from the AUV, whereas the WVAM method returns only a single estimate of flow velocity near, or at, the AUV. The reason for this is because the WVAM method measures the water column velocities by comparing the hydrodynamic forces acting on the vehicle, and these forces arise from the near AUV flow field. For example, the standard deviation between the ADCP and WVAM vertical water velocities at 0.5 m away from the AUV was 0.06 m s^{-1} and it increased up to 0.15 m s^{-1} at 9.5 m away from the vehicle. In turbulent environments, velocity fluctuations are typically larger and it is unlikely to have a single velocity value for a range of 10 m. Figure 7 illustrates the variation of the difference between ADCP and WVAM vertical water velocity magnitudes with the vertical distance from the AUV. A good correlation with variations less than around 0.08 m s^{-1} is seen until a vertical distance of around 4 m. Beyond 4 m, the difference increases up to around 0.3 m s^{-1}, showing that the WVAM method can be considered as accurate only in the vicinity of the vehicle.

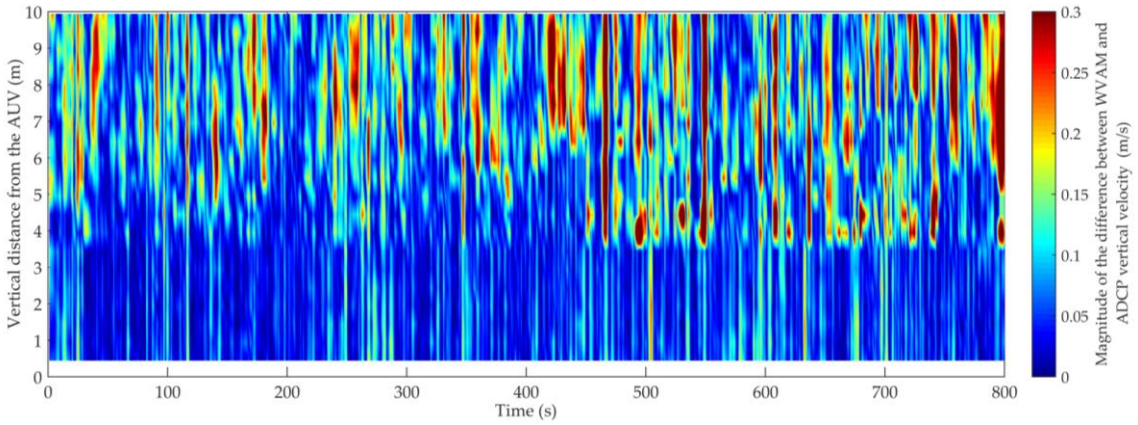

Figure 7. The variation of the difference between ADCP and WVAM vertical water velocity magnitudes with the vertical distance from the AUV.

Both WVAM and vehicle on-board ADCP measurements use the same Earth-referenced AUV velocities. Therefore, in order to further validate the WVAM method Randeni, Forrest, Cossu, Leong, King and Ranmuthugala [23] compared the WVAM estimations with those obtained from a stationary ADCP moored to the seabed. When the AUV was flying over the location of the stationary ADCP, it maintained an altitude of 11 m; hence, the ADCP water column velocities recorded from the bins at 11 m altitude were used for the comparison. The investigation was conducted using the same Gavia AUV at the same test location where the current study was carried out (i.e., Tamar estuary near the Batman Bridge). A good agreement between the two was observed with differences of 0.05 m s^{-1}, 0.08 m s^{-1}, and 0.01 m s^{-1} for the respective velocity components in the x, y, and z directions, further validating the WVAM method's ability to estimate flow velocities near, or at, the AUV and that the accuracy is independent of the vehicle velocities.

4.2. Length Scale of the WVAM Velocity Measurements

During the AUV field tests in the Tamar estuary, the motion response data of the vehicle were recorded at a rate of 0.87 Hz while the vehicle was travelling at an average forward speed of approximately 1.8 m s^{-1}. Hence, the data sampling distance was around 2.1 m (i.e., there was a horizontal distance of 2.1 m in between each data point). Therefore, the WVAM method neglects the velocity variations with length scales smaller than the data sampling distance. Also, the WVAM method assumes that the velocity components along the y and z axes are acting uniformly along the length of the AUV; i.e., the WVAM method estimates the mean velocity variation along the length of the AUV. Therefore, the smallest measurable length scale of the velocity variations in y and z axes is the data sampling distance or the length of the AUV, whichever is greater. In this case, the length of the AUV is approximately 2.7 m. However, the length scale of the velocity variations in the x axis is limited only by the data sampling distance. Hayes and Morison [2] estimated the vertical water velocity in the upper ocean by applying a Kalman filter to the AUV motion data. They reduced the measurement length scale down to half the AUV length by incorporating the phenomenon of pitching of the vehicle across a horizontal gradient of the vertical water velocity.

5. Recommendations

The WVAM method can be improved to capture the water velocity variations with length scales smaller than 2.7 m by overcoming the two limiting factors; i.e., the length of the AUV and the data sampling distance. The latter can be addressed by increasing the data sampling rate. Additionally, the scale restriction caused by the length of the AUV has to be resolved by identifying the variations of water velocities along the length of the AUV. This can be achieved by incorporating the difference between the vehicle angles of attack observed in the turbulent environment and that obtained from

the calm water simulation model (i.e., pitch angle difference for vertical water velocity gradient and the yaw angle for the horizontal gradient). The WVAM method can be further improved by incorporating a more accurate representation of the linear and non-linear hydrodynamic coefficients determined using techniques such as the captive model experiments and computational fluid dynamics simulations [24,25].

6. Conclusions

This study presents the WVAM method to estimate the flow velocity components of a turbulent water column, relative to the Earth, in x, y, and z axes of the AUV body-fixed coordinate system using the motion response of the vehicle. The water column velocities were determined by calculating the difference between the motion responses of the AUV observed in calm and turbulent water column conditions. The motion of the vehicle in the calm water environment was obtained by simulating the control commands executed during the field experiments conducted in the turbulent condition with a mathematical model that represents the calm water. The simulation model was developed within MATLAB Simulink and the associated hydrodynamic coefficients of the AUV were obtained using a recursive least squares system identification method.

The estimated water velocity components in x, y, and z direction agreed well with the measurements from the AUV's on-board ADCP with standard deviations of 0.09 m s^{-1}, 0.07 m s^{-1}, and 0.06 m s^{-1} for the respective components. These standard differences were well within the uncertainty margin of the ADCP results. WVAM velocity estimates were also compared with a bottom-mounted stationary ADCP data obtained while the AUV was flying over the stationary ADCP. Both datasets show good agreement with velocity differences of approximately 0.05 m s^{-1}, 0.08 m s^{-1}, and 0.01 m s^{-1} for the respective velocity components. An uncertainty analysis showed that the WVAM method estimates the respective velocity components within of $\pm$0.16 m s^{-1}, $\pm$0.16 m s^{-1}, and $\pm$0.15 m s^{-1}. The advantage of the proposed method is to determine velocity components closer to the vehicle where standard ADCPs are incapable of capturing the flow velocities due to their blanking distance. Estimating vertical and horizontal velocities around the boundary layer of the AUV is important to fill the blanking distance gap within a water column velocity profile, which is required for flow field characterization.

Acknowledgments: The authors would like to thank Rowan Frost (Research Engineer at Australian Maritime College, Uni. of Tasmania), Michael Underhill (Manager Technical Support at Australian Maritime College, Uni. of Tasmania), and David Box (Coxswain, Australian Maritime College, Uni. of Tasmania) for the kind support given during the AUV field experiments. The authors also thank Helgi Þorgilsson (Senior Systems Engineer at Teledyne Gavia) and Hordur Johannsson (Senior Software Engineer at Teledyne Gavia) for their continued technical support and assistance. This research did not receive any specific grant from funding agencies in the public, commercial, or not-for-profit sectors.

Author Contributions: The first author and all four co-authors were substantially involved in the design of the WVAM technique, its application and the analysis of the results. Randeni, Forrest, and Cossu were also involved in the AUV deployment and data acquisition while Leong, and Ranmuthugala contributed to the interpretation and modeling of the vehicle hydrodynamics. The final submitted version of the manuscript is approved by all authors.

Conflicts of Interest: The authors declare no conflict of interest.

Nomenclature

Symbol	Description	Unit
B	Buoyancy force of the AUV	(N)
C(v)	Coriolis-centripetal matrix	-
C_A(v)	Added mass component of C(v)	-
C_{RB}(v)	Rigid body force component of C(v)	-
D(v)	Damping matrix	-
g(η)	Vector of gravitational/buoyancy forces and moments	-
$H_{(t)}$	Matrix of time history of the states affecting the equations of motion	-

Symbol	Description	Unit
I_{xx}, I_{yy}, I_{zz}	Moments of inertia of the body about z, y, z axes, respectively	(kg m^2)
K, M, N	Hydrodynamic moment components relative to body axes	(Nm)
m	Mass of body	(kg)
M	System inertia matrix	-
M_A	Added mass component of M	-
M_{RB}	Rigid body force component of M	-
n	Number of time-steps	-
p, q, r	Angular velocity components relative to body axes x, y, z	(rad s^{-1})
$\dot{p}$, $\dot{q}$, $\dot{r}$	Angular acceleration components relative to body axes x, y, z	(rad s^{-2})
RPM	Propeller revolutions per minute	(-)
t	Time	(s)
u, v, w	Velocity components of origin of body along x, y and z directions	(m s^{-1})
$\dot{u}$, $\dot{v}$, $\dot{w}$	Acceleration components of origin of body along x, y and z directions	(m s^{-2})
W	Dry weight of the vehicle in air	(N)
x	The longitudinal axis, directed from the after to the forward end of the body	-
X, Y, Z	Hydrodynamic force components relative to body axes	(N)
x_g, y_g, z_g	Coordinates of center of mass relative to body axes	(m)
y	The transverse axis, directed to starboard	-
$y_{(t)}$	Next step state history for the equation of interest	-
z	The normal axis, directed from top to bottom	-
θ, ψ, ϕ	Angles of pitch, yaw and roll, respectively	(Rad)
$\vec{\eta}$	Vector of position and Euler angles (i.e., [x, y, z, φ, θ, ψ])	
$\tau_{control}$	Vector of propulsion and control surface forces and moments	-
$\vec{\nu}$	Velocity vector (i.e., [u, v, w, p, q, r]^T)	-
$\vec{\nu}_{AUV(calm)}$	linear velocity vector of the AUV (relative to the earth, in the body-fixed Coordinate system) obtained from the calm water simulation model when the control commands recorded during the field tests were simulated	(m s^{-1})
$\vec{\nu}_{AUV(turbulent)}$	Linear velocity vector of the AUV (relative to the earth, in the body-fixed coordinate system) measured in the turbulent environment	(m s^{-1})
$\vec{\nu}_{water}$	Linear velocity vector of the surrounding water column (along the x, y and z directions) relative to the earth in the body-fixed coordinate system	(m s^{-1})
$\Theta_{(t)}$	Parameter vector to be identified	-
$\vec{\nu}_{water(ADCP)}$	Water column velocity measured using the ADCP	(m s^{-1})
$\vec{\nu}_{water(WVAM)}$	Water column velocity estimated using the WVAM method	(m s^{-1})

References

1. Hughes, M.G.; Masselink, G.; Brander, R.W. Flow velocity and sediment transport in the swash zone of a steep beach. *Mar. Geol.* **1997**, *138*, 91–103. [CrossRef]
2. Hayes, D.R.; Morison, J.H. Determining turbulent vertical velocity, and fluxes of heat and salt with an autonomous underwater vehicle. *J. Atmos. Ocean. Technol.* **2002**, *19*, 759–779. [CrossRef]
3. Simpson, M.R. *Discharge Measurements Using a Broad-Band Acoustic Doppler Current Profiler*; US Department of the Interior, US Geological Survey: Sacramento, CA, USA, 2001.
4. Sprintall, J.; Gordon, A.L.; Flament, P.; Villanoy, C.L. Observations of exchange between the South China Sea and the Sulu Sea. *J. Geophys. Res. Oceans* **2012**, *117*. [CrossRef]
5. Fong, D.A.; Jones, N.L. Evaluation of auv-based adcp measurements. *Limnol. Oceanogr. Methods* **2006**, *4*, 58–67. [CrossRef]
6. Kimura, S.; Jenkins, A.; Dutrieux, P.; Forryan, A.; Naveira Garabato, A.C.; Firing, Y. Ocean mixing beneath Pine Island Glacier ice shelf, West Antarctica. *J. Geophys. Res. Oceans* **2016**, *121*, 8496–8510. [CrossRef]
7. Gandhi, B.; Verma, H.; Patnaik, S. Discharge measurement in small hydropower stations using acoustic doppler current profiler. In Proceedings of the 7th International Conference on Hydraulic Efficiency Measurements, IGHEM-2008, Milan, Italy, 3–6 September 2008; pp. 3–6.

8. Frajka-Williams, E.; Eriksen, C.C.; Rhines, P.B.; Harcourt, R.R. Determining vertical water velocities from seaglider. *J. Atmos. Ocean. Technol.* **2011**, *28*, 1641–1656. [CrossRef]
9. Rudnick, D.L.; Johnston, T.; Sherman, J.T. High-frequency internal waves near the luzon strait observed by underwater gliders. *J. Geophys. Res. Oceans* **2013**, *118*, 774–784. [CrossRef]
10. Forrest, A.; Trembanis, A.; Todd, W. Ocean floor mapping as a precursor for space exploration. *J. Ocean Technol.* **2012**, *7*, 69–86.
11. Kim, K.; Ura, T. Fuel-optimal guidance and tracking control of auv under current interaction. In Proceedings of the Thirteenth International Offshore and Polar Engineering Conference, Honolulu, HI, USA, 25–30 May 2003; International Society of Offshore and Polar Engineers: Mountain View, CA, USA, 2003.
12. Lee, G.R. *Principles of Operation a Practical Primer*; RD Instruments: San Diego, CA, USA, 1996. Available online: http://RDInstruments.com (accessed on 20 August 2016).
13. Green, S.; Cossu, R.; Penesis, I.; Nader, J.-R. Tidal energy: A promising future resource for tasmania. In Proceedings of the 3rd Asian Wave and Tidal Energy Conference (AWTEC 2016), Singapore, 24–28 October 2016; Research Publishing: Singapore, 2016; pp. 891–898.
14. Ananthakrishnan, P.; Zhang, K.-Q. Auv motion in a wave field. In Proceedings of the OCEANS'98, Nice, France, 28 September–1 October 1998; pp. 1059–1063.
15. Steel, V. *Investigation Into the Effect of Wave Making on a Submarine Approaching the Free Surface*; University of Tasmania: Launceston, Australia, 2010.
16. Fossen, T.I. *Handbook of Marine Craft Hydrodynamics and Motion Control*; John Wiley & Sons: Chichester, UK, 2011.
17. Prestero, T.T.J. Verification of a Six-Degree of Freedom Simulation Model for the Remus Autonomous Underwater Vehicle. Master's Thesis, Massachusetts Institute of Technology, Cambridge, MA, USA, September 2001.
18. SNAME. *Nomenclature for Treating the Motion of a Submerged Body Through a Fluid*; Technical and Research Bulletin No. 1–5; SNAME: New York, NY, USA, 1952.
19. Fossen, T.I. *Guidance and Control of Ocean Vehicles*; John Wiley & Sons: Chichester, UK, 1994.
20. Thorgilsson, H. Control of a Small Undermanned Underwater Vehicle Using Zero Optimizing Controllers. Master's Thesis, Department of Electrical and Computer Engineering, University of Iceland, Reykjavík, Iceland, October 2006.
21. Ljung, L. *System Identification: Theory for the User*; PTR Prentice Hall: Englewood Cliffs, NJ, USA, 1999.
22. Wolkerstorfer, W.J. A Linear Maneuvering Model for Simulation of Slice Hulls. Master's Thesis, DTIC Document. Naval Postgraduate School, Monterey, CA, USA, 1995.
23. Randeni, S.A.T.; Forrest, A.L.; Cossu, R.; Leong, Z.Q.; King, P.D.; Ranmuthugala, D. Autonomous underwater vehicle motion response: A nonacoustic tool for blue water navigation. *Mar. Technol. Soc. J.* **2016**, *50*, 17–26. [CrossRef]
24. Randeni, S.A.T.; Leong, Z.; Ranmuthugala, D.; Forrest, A.; Duffy, J. Numerical investigation of the hydrodynamic interaction between two underwater bodies in relative motion. *Appl. Ocean Res.* **2015**, *51*, 14–24.
25. Phillips, A.B. Simulations of a Self Propelled Autonomous Underwater Vehicle. Ph.D. Thesis, University of Southampton, Southampton, UK, April 2010.
26. Hildebrandt, M.; Hilljegerdes, J. Design of a versatile auv for high precision visual mapping and algorithm evaluation. In Proceedings of the 2010 IEEE/OES on Autonomous Underwater Vehicles (AUV), Monterey, CA, USA, 1–3 September 2010; pp. 1–6.